MNRAS **000**, 1–?? (2015) Preprint 5th May 2016 Compiled using MNRAS LATEX style file v3.0

Galaxy gas as obscurer: II. Separating the galaxy-scale and nuclear obscurers of Active Galactic Nuclei

Johannes Buchner, [1,2]⋆ Franz Bauer[1,2], [EAGLE collaborators]
[1] *Millenium Institute of Astrophysics, Vicuña. MacKenna 4860, 7820436 Macul, Santiago, Chile*
[2] *Pontificia Universidad Católica de Chile, Instituto de Astrofísica, Casilla 306, Santiago 22, Chile*

Accepted XXX. Received YYY; in original form ZZZ

ABSTRACT

The "torus" obscurer of Active Galactic Nuclei, is poorly understood in terms of its density, substructure and physical mechanisms. Large X-ray surveys provide model boundary constraints, for both Compton-thin and Compton-thick levels of obscuration, as obscured fractions are mean covering factors $f_{\rm cov}$. However, a major remaining uncertainty is host galaxy obscuration. In Paper I we discovered a relation of $N_{\rm H} \propto M_\star^{1/3}$ for the obscuration of galaxy-scale gas. Here we apply this observational relation to the AGN population, and find that galaxy-scale gas is responsible for a luminosity-independent fraction of Compton-thin AGN, but does not produce Compton-thick columns. With the host galaxy obscuration understood, we present a model of the remaining, nuclear obscurer which is consistent with a range of observations. The PuffedTorus model consists of a Compton-thick component ($f_{\rm cov} \sim 35\%$) and a Compton-thin component ($f_{\rm cov} \sim 40\%$), which is present depending on black hole mass and luminosity. This is a useful summary of observational constraints for torus modellers who would like to reproduce this behaviour. It can also be employed as a sub-grid recipe in cosmological simulations which do not resolve the torus. We also investigate host-galaxy X-ray obscuration inside cosmological, hydro-dynamic simulations (EAGLE, Illustris). The obscuration from ray-traced galaxy gas can be in agreement with observations, but is highly sensitive to the chosen feedback assumptions.

1 INTRODUCTION

The vast majority of Active Galactic Nuclei (AGN) are obscured by thick columns of gas and dust. X-ray surveys over the last decade indicate that $20-40\%$ are hidden behind Compton-thick column densities ($N_{\rm H} \gtrsim 10^{24}{\rm cm}^{-2}$) and of the remaining population, $\sim 75\%$ are obscured with $N_{\rm H} = 10^{22} - 10^{24}{\rm cm}^{-2}$ (e.g. Treister et al. 2004; Brightman et al. 2014; Ueda et al. 2014; Buchner et al. 2015; Aird et al. 2015) at the peak of AGN activity at redshift $z = 0.5-3$. An open question is whether the same gas reservoir is responsible for fuelling the AGN by accretion onto Supermassive Black Holes (SMBHs), and whether it itself is affected by AGN activity. To address this, the first step is to identify the scale at which the obscuring gas resides. Traditionally, AGN obscuration is associated with the "torus", a nuclear ($\sim$ 10pc) structure around the accretion disk. Many basic questions about this gas reservoir remain to be answered, including its density, substructure and stability mechanism (Elitzur 2006; Hoenig 2013). Assuming sampling from random viewing angles, the large fraction of obscured AGN implies large covering fractions. Therefore turbulent structures such as winds from accretion disks have been invoked. However, for the covering fractions to be useful constraints for torus models, the importance of galaxy-scale gas to the obscuration has to be estimated. Separating the covering and column densities from nuclear and galaxy-scale obscurers is the goal of this work.

Local galaxies exemplify that several scales can contribute to the obscured columns. The Milky Way gas distribution shows column densities of $N_{\rm H} > 10^{22}{\rm cm}^{-2}$, but only in very low Galactic latitudes ($|b| \lesssim 2°$, Dickey & Lockman 1990; Kalberla et al. 2005). Towards the Galactic Center columns with $N_{\rm H} > 10^{24}{\rm cm}^{-2}$ can be found in the Central Molecular Zone (Morris & Serabyn 1996; Molinari et al. 2011), as well as in the equivalent central zones of nearby AGN host galaxies (Prieto et al. 2014). Also the obscuration in the AGN host galaxy NGC 1068 is clearly nuclear (in this work: $\sim$ 100pc or smaller), because its Compton-thick column is observed in a face-on galaxy (Matt 1997). On the other hand, many nearby, obscured AGN are hosted in edge-on galaxies (Maiolino & Rieke 1995), which suggests that dust-lanes may also be important obscurers (see also Goulding & Alexander 2009, for galactic optical/infrared extinction). Hence Matt (2000) proposed a two-phase model for the obscuration of AGN: a central, nuclear obscurer which provides Compton-thick obscuration, and the host galaxy, which provides mildly obscured lines of sight.

However, the Milky Way and local galaxies are limited in their use as templates for the high-redshift universe, specifically at peak SMBH growth ($z = 0.5-3$; e.g., Aird et al.

2010). At that time, the gas content in galaxies was probably higher, as indicated by molecular gas measurements (e.g. Tacconi et al. 2013) which perhaps lead to the peak of star formation (see review by Madau & Dickinson 2014) and the increase in the fraction of obscured AGN with redshift (e.g. Treister et al. 2004; Ueda et al. 2014; Buchner et al. 2015). The efficient growth of SMBHs at these early epochs has been attributed to galaxy mergers (Ciotti & Ostriker 2001). This model was expanded by Hopkins et al. (2006) to reproduce local scaling relationships between galaxy components and SMBH masses, the luminosity function of AGN, the fraction of active galaxies, and the obscuration dichotomy of AGN. The evolutionary model also explains why bright AGN are less frequently found to be mildly obscured than faint AGN (Ueda et al. 2003; Silverman et al. 2008; Ebrero et al. 2009; Ueda et al. 2014; Buchner et al. 2015; Aird et al. 2015), albeit only qualitatively (Hopkins et al. 2005a, 2006). In this work we investigate the obscuring role of galaxy-scale gas in the transition from obscured AGN in gas-rich galaxies to unobscured AGN in gas-poor galaxies, as proposed in the evolutionary sequence of that model. To effectively decouple the galaxy-scale and nuclear X-ray obscurer, we need to go beyond a single, central source.

This paper is organised as follows: In Section 2 we present our computation of the galaxy-scale obscuration using observational results from Paper I of the obscuring column distribution of galaxies, applied to the AGN population. Section 3 presents our results, which we discuss in Section 4. With the galaxy-scale obscurer subtracted, we present a model for the remaining nuclear obscurer in Section 4.2.

Independently, Section 5 looks into simulated galaxies in hydro-dynamic cosmological simulations. These provide predictions for the amount of gas inside galaxies, from which we derive obscured fractions using ray-tracing. Various model uncertainties are discussed. Finally we summarise our conclusions in Section 6.

2 METHODOLOGY

Our goal is to predict the fraction of obscured AGN from the obscuration of host galaxy-scale gas alone, i.e. without nuclear obscuration (the torus and central molecular zones). In this fashion we will be able to separate the large-scale and small-scale obscurer. In Paper I we established a relation between the distribution of X-ray absorbing column densities, $N_{\rm H}$, in galaxies and the stellar mass of the galaxy. It follows approximately a normal distribution around

$$N_{\rm H} = 10^{21.7}{\rm cm}^{-2} \times \left(M_\star/10^{9.5}M_\odot\right)^{1/3} \quad (1)$$

with standard deviation $\sigma = 0.5\,$dex. This $N_{\rm H} - M_\star$ relation was derived using an unbiased sample of long Gamma Ray Bursts (LGRBs). Since the obscuration is host mass dependent, the obscurer is arguably the host galaxy itself. In Paper I we show that modern cosmological hydro-dynamic simulations reproduce absorption by galaxy-scale metal gas and predict $N_{\rm H} - M_\star$ relations very similar to Equation 1.

We apply this relation to the AGN host galaxy population to estimate host galaxy obscuration. This relation was derived from actively star forming galaxies, therefore a caveat is that results may slightly over-represent the galaxy gas present in AGN host galaxies which have average (Rosario et al. 2011, 2013; Santini et al. 2012) or even below-average (Mullaney et al. 2015) star formation rates. The major benefit of using this relationship is that it is based on the same observable as AGN obscured fractions, namely the photo-electric absorption of X-rays. Paper I also investigated the host galaxy metallicity bias of LGRB and concluded that it has a negligible effect on the obscurer. Local galaxies are also shown there to follow the $N_{\rm H} - M_\star$ relation.

We start with the stellar mass function (SMF) of the galaxy population. Its shape $P(M_\star|z)$ is approximately a Schechter function and was measured by e.g. Muzzin et al. (2013) and Ilbert et al. (2013) out to $z \sim 4$. Then we populate the galaxies with AGN. The occupation probability $P({\rm AGN}|M_\star, z)$ has been measured by Aird et al. (2012) and Bongiorno et al. (2012) primarily for the redshift interval $z = 0.5 - 2$. More accurately, these authors measure the specific accretion rate distribution (SARD), $P(L_{\rm X}|M_\star, z)$, where $L_{\rm X}$ is the $2 - 10\,$keV X-ray luminosity. They find factorised powerlaw relationships of the form $P(L_{\rm X}|M_\star, z) = A \cdot L_{\rm X}^{\gamma_L} \cdot M_\star^{\gamma_M} \cdot (1+z)^{\gamma_z}$. At the highest luminosities, an Eddington limit is required to explain the steep decrease of the luminosity function (Aird et al. 2013). In this work, however, we focus on the luminosity range $L_{\rm X} = 10^{42-45}{\rm erg/s}$ regime and thus use only the observed relation. The final ingredient is the obscuring column density distribution (CDD) $P(N_{\rm H}|M_\star)$, which is given by Equation 1 as a normal distribution in $\log N_{\rm H}$. We assume that the galaxy-scale gas is independent of nuclear activity for individual galaxies.

The obscured fraction can then be simply computed by Monte Carlo simulations. Analytically we can put the three distributions together as

$$P(N_{\rm H}, L_{\rm X}, M_\star|z) = \underbrace{P(M_\star|z)}_{\rm SMF} \times \underbrace{P(L_{\rm X}|M_\star, z)}_{\rm SARD} \times \underbrace{P(N_{\rm H}|M_\star)}_{\rm Eq\ 1} \quad (2)$$

After inserting the factorised powerlaw relationship of the SARD, the result has the form

$$P(N_{\rm H}, L_{\rm X}, M_\star|z) = A \times L_{\rm X}^{\gamma_L} \times f(M_\star|z) \times P(N_{\rm H}|M_\star). \quad (3)$$

While the absolute probability of finding an AGN is a function of luminosity, the mass distribution is independent of luminosity. That is, at every luminosity (not considering the Eddington limit), the same mix of host stellar masses contribute. Therefore, the implication is that the obscuration due to host galaxy-scale gas is the same at all AGN luminosities.

We adopt an AGN definition of $L_{\rm X} > 10^{42}{\rm erg/s}$. The frequency distribution of column densities $N_{\rm H}$ for the AGN population is then computed by integrating over stellar mass and luminosity:

$$P(N_{\rm H}|z) = \int\int_{10^{42}{\rm erg/s}}^{\infty} P(N_{\rm H}, L_{\rm X}, M_\star|z)\, dL_{\rm X}\, dM_\star. \quad (4)$$

Finally the obscured AGN fraction is the cumulative distribution, i.e. the frequency of AGN being covered by a

certain column density threshold $N_{\rm H}$ or higher:

$$f_{\rm cov}(> N_{\rm H}) = \int_{N_{\rm H}}^{\infty} P(N_{\rm H}'|z) dN_{\rm H}'. \quad (5)$$

Into the calculation of $f_{\rm cov}$ we propagate the uncertainties from the obscuration relation for Paper I. We consider two SMF (Muzzin et al. 2013 and Ilbert et al. 2013) and two SARD measurements (Aird et al. 2012 and Bongiorno et al. 2012), to incorporate systematic uncertainties. To summarise, we rely only on observational relations to predict the obscuration of the AGN population by galaxy-scale gas.

3 RESULTS

The obscured fraction of the AGN population from putting together the observed relationships are shown in Figure 1. Each panel represents a specific redshift. Red lines show our fraction of obscured AGN (y-axis) for a given column density $N_{\rm H}$ (x-axis), assuming various SMF and SARDs, with shades showing the uncertainties stemming from the obscuration relation.

Firstly, galaxy-scale gas does not provide Compton-thick column densities ($N_{\rm H} > \sigma_T^{-1} = 1.5 \times 10^{24} {\rm cm}^{-2}$). This is because massive galaxies which reach those densities are rare and therefore represent a negligible fraction of the AGN population. In contrast, the observed fraction of Compton-thick AGN is $\sim 38\%$ (see Buchner et al. 2015 and references therein). We can conclude that Compton-thick obscuration is always associated with the nuclear region. An alternative, theoretical argument based on the total metal gas mass present in galaxies is laid out in Appendix A and arrives at the same conclusion.

We therefore focus on the Compton-thin obscurer and compare our obscuration results to the fraction of Compton-thin AGN with $N_{\rm H} > 10^{22} {\rm cm}^{-2}$, a common definition of "obscured" AGN. This step implicitly assumes that the Compton-thick nuclear obscurer is randomly oriented with respect to the galaxy, in accordance with chaotic accretion (King & Pringle 2006).

We now compare to measurements of the obscured fraction of Compton-thin AGN from surveys. When these fractions are treated as covering fractions, they contain both galaxy-scale obscuration and nuclear obscuration. Therefore the data points should always be understood as upper limits to the galaxy-scale gas obscuration. Figure 1 shows results from surveys at the peak of the accretion history ($z = 1 - 3$ panels) from Ueda et al. (2014) and Buchner et al. (2015), as well as surveys which include the local Universe (Burlon et al. 2011; Ueda et al. 2014; Aird et al. 2015; Ricci et al. 2016). Two cases are important: (1) the fraction of obscured AGN at the bright end ($L_{\rm X} \geq 10^{45} {\rm erg/s}$), where the lowest obscured fractions are observed ($f_{\rm bright} \sim 40\%$, shown as triangles), and (2) at the faint end ($L_{\rm X} \sim 10^{43} {\rm erg/s}$), where the highest obscured fractions are observed ($f_{\rm faint} \sim 75\%$, shown as squares). Our results are, as discussed in Section 2, luminosity-independent. When comparing the triangle data points at $N_{\rm H} = 10^{22} {\rm cm}^{-2}$ in Figure 1 representing the bright end to our results (red), we find broad agreement within two-sigma uncertainties (red shades). However, due to the large uncertainties also the faint end may be in agreement. Therefore we can not distinguish whether galaxy-scale obscuration decreases toward the bright end, or increases toward the faint end. Nevertheless we can conclude that galaxy-scale obscuration is an important, if not dominant, AGN obscurer at $N_{\rm H} = 10^{22-23} {\rm cm}^{-2}$. At higher column densities, e.g. $N_{\rm H} = 10^{23.5} {\rm cm}^{-2}$, the observed obscured fraction is clearly higher than our results from galaxy-scale gas. Therefore a nuclear obscurer is necessary to explain the elevated data points. The shape of the distribution is driven by the Gaussian distribution of the $N_{\rm H} - M_\star$ relation, a shape assumed in Paper I to fit the dispersion. Adopting a different distribution, would flatten the tails and permit unobscured LOS.

Note that our results are meaningful for the AGN population – the obscuration of individual host galaxies is stellar-mass dependent with substantial variations between individual galaxies (see Equation 1).

4 DISCUSSION

Our main result is that the host galaxy gas provides a luminosity-independent obscurer, for which we compute covering fractions. This obscurer does not provide Compton-thick columns, but large covering fractions ($40 - 90\%$) at $N_{\rm H} > 10^{22} \, {\rm cm}^{-2}$. These high covering fractions suggest that a substantial part of the type1/type2 dichotomy is due to galaxy-scale gas. This is consistent with the finding of Maiolino & Rieke (1995) that nearby type2 AGN are often edge-on galaxies. We note that our results tend to produce high covering fractions, which are only consistent with the measurements due to large uncertainties. We speculate that the use of GRB host galaxies in Paper I may slightly bias our results when applied to AGN host galaxies. GRB host galaxies are currently star forming and thus may have slightly more gas than the average AGN galaxy (see caveats discussed in Section 2). A correction in the column density by a factor of 2 would agree well with data points at all redshifts. This is demonstrated by the dashed line in Figure 1, which shows a normal distribution around $\log N_{\rm H}/{\rm cm}^{-2} = 10^{22}$ with width 0.5. Nevertheless, our results are consistent with the current AGN surveys.

Our results give, for the first time, constraints on the galaxy-scale obscurer alone. We use this in the following sections to disentangle the AGN nuclear obscurer from the galaxy-scale obscurer (Section 4.1), and to describe their behaviour as a function of accretion luminosity, host galaxy stellar mass and redshift (Section 4.2). Finally physical effects leading to this behaviour are discussed in Section 4.3.

4.1 Luminosity-dependence of AGN obscuration

We can now discuss the luminosity-dependence of the obscurer. X-ray surveys consistently find a strong decline towards high luminosities (Ueda et al. 2003; Hasinger et al. 2005; La Franca et al. 2005; Ebrero et al. 2009; Ueda et al. 2014; Buchner et al. 2015; Aird et al. 2015) of the obscured fraction $N_{\rm H} > 10^{22} \, {\rm cm}^{-2}$ in the Compton-thin AGN (CT-NAGN) population. In Figure 2 we have sketched this decline from $\sim 70\%$ to a persistent $\sim 40\%$. According to our results, this can be interpreted as two scales contributing to the obscuration: a 40% galaxy-scale obscurer, and a

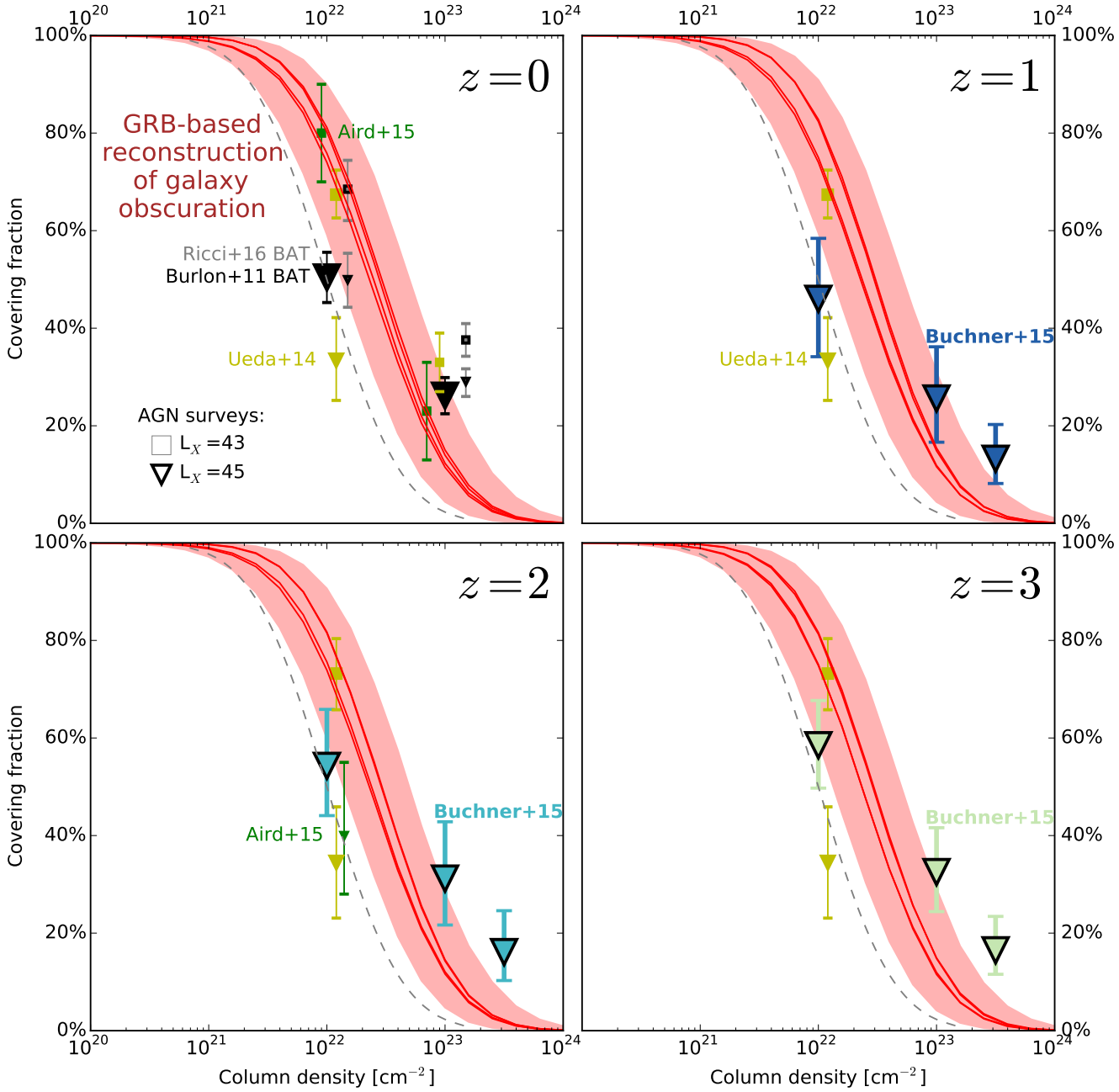

Figure 1. Galaxy-scale obscuration of AGN. At various redshift intervals we show the fraction of AGN (y-axis) that is covered by a given column density $N_{\rm H}$ (x-axis). Red lines indicate our derivations with uncertainties shown in red shades. Galaxy-scale obscuration is negligible for column densities of 10^{24}cm^{-2}, but a important contributor to the AGN fraction at $N_{\rm H} \approx 10^{22-23}$ cm^{-2}. Data points represent fractions from AGN surveys: Bright AGN (large triangles) show lower obscurations than faint AGN (squares). The data points are black, yellow, green small symbols (Ueda et al. 2014; Aird et al. 2015; Ricci et al. 2016, respectively) and black and coloured large triangles (Burlon et al. 2011; Buchner et al. 2015, respectively). Since AGN also have a nuclear obscurer, these should be regarded as upper limits for galaxy gas obscuration (red). Arguable consistent with all data points is a normal distribution around 10^{22}cm^{-2} (dashed grey curve), which is kept constant across panels.

luminosity-dependent nuclear obscurer. The former is constrained from GRB observations (Paper I), re-weighted to the mass distribution of AGN (results of this paper). The latter is the remainder to fit the observations. According to this picture, the nuclear obscurer completely disappears toward high luminosities at $L(2-10\,{\rm keV}) \approx 10^{44.5}$erg/s. This luminosity is however redshift-dependent, with higher redshifts having higher cut-off luminosities. This has been found in many works (Ueda et al. 2003; Ebrero et al. 2009; La Franca et al. 2005; Ueda et al. 2014; Aird et al. 2015) by fitting a empirical, parametric model to the relative number density derived from AGN surveys. Buchner et al. (2015) derived the same result using a non-parametric method, indicating that this is indeed a robust result. In Buchner et al.

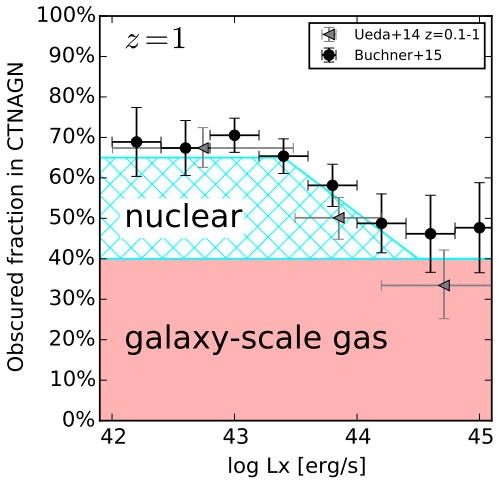

Figure 2. The observed luminosity-dependence of the obscured fraction. With the galaxy-scale gas obscuration constrained and luminosity-independent (red, Section 3), we separate out the nuclear, variable obscurer (cyan) and create a luminosity-dependent model (Section 4.2).

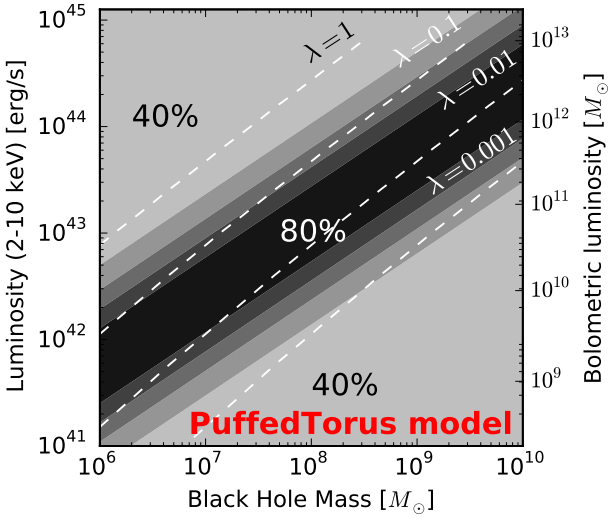

Figure 3. Covering fractions as a function of accretion luminosity and mass of the proposed PuffedTorus model. Dashed lines indicate constant Eddington accretion rates. At intermediate accretion rates, the torus is puffed up and covers large fractions of the black hole.

(2015), the implications for obscurer models were discussed in their Section 5.3. They concluded that an Eddington-limited blow-out of the obscurer could explain the luminosity dependence. As the luminosity dependence is observed to evolve, a black hole mass dependence needed to be invoked. Under the assumption of black hole mass downsizing, i.e., that the average accreting black hole is more massive at high redshift than at low redshift, the turn-over luminosity decreases over cosmic time. Black hole mass downsizing has evidence from optical observations of the black hole mass function evolution (Schulze & Wisotzki 2010; Kelly & Shen 2013; Schulze et al. 2015) and semi-analytic models which reproduce the evolution of the AGN luminosity function (Fanidakis et al. 2012; Enoki et al. 2014; Hirschmann et al. 2014). Recently, Oh et al. (2015) found evidence that the type-1 fraction in a SDSS selected sample is both luminosity and black hole mass dependent.

4.2 PuffedTorus - a unified obscurer model

Since neither semi-analytic nor hydro-dynamic cosmological simulations can resolve the nuclear obscurer of AGN, we present a sub-grid model for post-processing. The PuffedTorus model has few parameters and is constructed so that it reproduces the fraction of obscured AGN as a function of redshift and luminosity as discussed above. It can also serve as a summary of observational constraints when exploring physical models for the obscurer.

We assume that a nuclear Compton-thick obscurer covers a fraction of the SMBH, $f_{\rm CT} \sim 35\%$. Evidence for this number comes directly from AGN surveys (Buchner et al. 2015), matching the soft and hard X-ray luminosity function (Aird et al. 2015) and matching the Compton-thin X-ray luminosity function to the spectrum of the Cosmic X-ray background (Ueda et al. 2014). Similar fractions are now also found in local surveys, e.g. Ricci et al. (2016).

We propose that the remaining Compton-thin sky is obscured by galaxy-scale gas as well as a nuclear Compton-thin obscurer according to the formula:

$$f_{\rm cov} = f_{\rm gal} + f_{\rm nuc} \cdot \exp\left\{-\frac{1}{2\sigma^2}\left(\log\frac{L}{L_{\rm peak}}\right)^2\right\} \quad (6)$$

The luminosity-independent obscuration, $f_{\rm gal}$ is on average $\sim 40\%$. In hydro-dynamic simulations it can be derived for individual galaxies through ray-tracing (see Section 5), or otherwise calculated from Equation 1. The obscuration of Equation 6 reaches a average maximum of 75% at luminosity $L_{\rm peak}$ (see Figure 2), and we therefore suggest $f_{\rm nuc} = 35\%$. We chose a Gaussian form which requires fewer parameters than a linear decline (e.g. Ueda et al. 2014). The obscured fraction declines towards both bright and faint ends to $f_{\rm gal}$ with characteristic width of the transition defined by σ. Evidence for the low-luminosity decline was found in surveys of the local Universe (Burlon et al. 2011; Brightman & Nandra 2011) as well as at high redshifts (Buchner et al. 2015).

As motivated in the above Section 4, the peak luminosity $L_{\rm peak}$ is in turn a function of mass:

$$\frac{L_{\rm peak}}{10^{43}{\rm erg/s}} = \left(\frac{M_{\rm BH}}{M_{L43}}\right)^p$$

Here, at M_{L43} the distribution peaks at $L(2-10\,{\rm keV}) = 10^{43}{\rm erg/s}$, which is $L_{\rm bol} = 10^{10.7} L_{\odot}$ using the conversion of (Marconi et al. 2004). The mass-dependence is defined by the p parameter: at $p = 0$, the PuffedTorus is mass-independent, corresponding to a strict luminosity-dependent unified model, while at $p = 1$ it is only Eddington-rate dependent. The parameters p, M_{L43} and σ are not known apriori. For mass-scaling, $p = 2/3$ is suggested from the theoretical works on the obscurer by Elitzur & Netzer (2016) and Wada (2015), however a wide range (e.g. $p = 0 - 2$) may be considered (see also Hönig & Beckert 2007). We de-

Table 1. Parameters of the PuffedTorus model. The recommended values are constrained by local observations as described in Section 4.2.

Parameter	Symbol	Observed Range	Recommended Value
Compton-thick fraction	$f_{\rm CT}$	20% - 40%	35% (fixed)
Host galaxy obscuration	$f_{\rm gal}$	0% - 60%	galaxy-dependent, but 40% on average
Compton-thin stirred obscuration	$f_{\rm nuc}$	30% - 50%	35%
Luminosity-dependence width	σ	0 - 1	0.5
Reference mass	M_{L43}	10^7- $10^8 M_\odot$	$10^{7.87} M_\odot$
Mass-dependence	p	0 - 2	2/3 (consider also 0, 1, 4/3)
Intrinsic luminosity $(2-10\,\mathrm{keV})$	L	(dynamic)	Determined from accretion rate using bolometric corrections of Marconi et al. (2004)

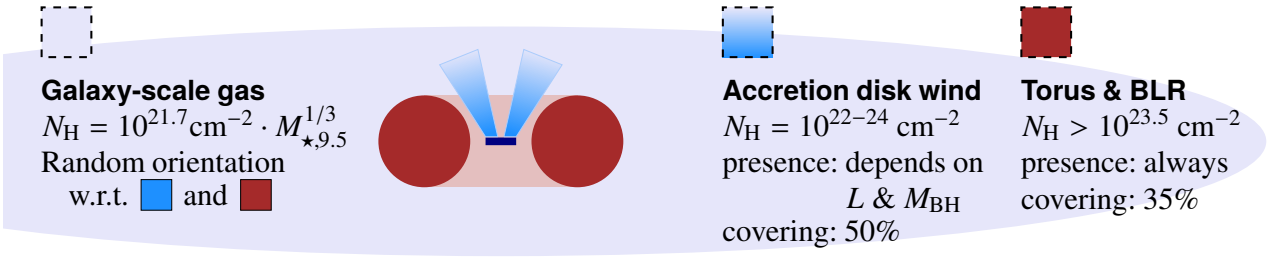

Figure 4. Cartoon of the three known obscurer components: Galaxy-scale obscuration (light blue), luminosity-dependent nuclear obscuration (blue) and Compton-thick nuclear obscuration (red). In this illustration, the disappearing Compton-thin obscurer is provided by a clumpy accretion disk wind, while the Compton-thick obscurer is a clumpy donut-like structure. Both are embedded in the host galaxy under random orientation. This is one scenario appropriate for the proposed PuffedTorus model.

rive fiducial values for the other two parameters using the Swift/BAT survey of local AGN. That survey reported a mean mass of $\log M_{\rm BH}/M_\odot = 7.87$ with a standard deviation of 0.66 dex and a skew towards low masses (Winter et al. 2009). Adopting an appropriate skewed normal distribution with skew parameter -10 (tail to low masses) around $M_{L43} = 10^{7.87} M_\odot$, we find that $\sigma \approx 0.5$ approximately reproduces the width of the obscured fraction function reported in Burlon et al. (2011), and peaks at $L_{\rm X} = 10^{43}$erg/s. Table 1 lists the parameters of the PuffedTorus model, with recommended typical values. We emphasise that the observations pertaining the redshift evolution have not been used when constructing our model. Cosmological simulations using the PuffedTorus model can thus compare against those (e.g. Buchner et al. 2015).

The ratio of dust re-radiated infrared luminosity to bolometric, illuminating luminosity has been used to measure the irradiated area (obscurer covering factor) of individual AGN. Surveys employing this method (e.g. Maiolino et al. 2007; Lusso et al. 2013) typically find, once corrected for anisotropic illumination and emission (Stalevski et al. 2016, see their Figure 13), fractions between 40% and 75% (luminosity-dependent). Those measurements would include emission from the Compton-thick obscurer and the nuclear, Compton-thin obscurer. With our assumed fiducial values we obtain 35% ($f_{\rm CT}$) to 75% ($f_{\rm CT} + f_{\rm nuc}$) and are therefore also in agreement with those observations. Infrared studies remain however difficult to use as a constraint as the entire infrared SED has to be constrained for each object (Netzer et al. 2016) and covering factors have to be corrected based on uncertain model geometries (Stalevski et al. 2016).

Figure 3 illustrates the behaviour of the PuffedTorus model. The obscured fraction undergoes a luminosity and mass-dependent peak, where the Compton-thin medium is extended and occupies a substantial fraction of the sky. Due to the host galaxy, a constant fraction is present at all luminosities and masses. The Compton-thick fraction here has been assumed to be constant, albeit we note that Ricci et al. (2016) claims a luminosity-dependence of the Compton-thick fraction.

4.3 Physical obscurer processes

Physical processes giving rise to the luminosity and mass-dependent behaviour can not be discussed rigorously within the scope of this paper. However, we point out a few key results of recent theoretical works. Otherwise we refer to the review of Hoenig (2013) which discusses current torus modelling approaches.

We take note of the analytic wind model formalism described in Elitzur & Netzer (2016) and of the radiation-driven fountain model by Wada (2015). Both models produce a vertically extended obscurer structure as a function of luminosity and mass. At low luminosities, radiation is not sufficient to puff up the obscurer. In the hydro-dynamical simulations of Wada (2012) very high accretion luminosities are associated with strong outflows, which suppress the vertical extent of the obscuring structure as they occupy larger angles. The cartoon of Figure 4 illustrates such a possible wind scenario for the three, distinct obscuring components, with approximately the correct opening angles. For visualisation we have smooth gas distributions, while in reality the obscurer is thought to be clumpy (see e.g., Markowitz et al. 2014, and references therein). To date, models of the nuclear obscurer largely lack observational constraints. Our PuffedTorus model summarises observational boundary constraints of covering fractions and column densities for how a physical "torus" model should behave.

A further, commonly overlooked aspect is the evolution of AGN. Faint AGN are much more common than luminous AGN (e.g. Barger & Cowie 2005; Ueda et al. 2003; Aird et al. 2010), a fact that has to be explained with the triggering and light-curve of accretion events. Galaxy-galaxy mergers are today thought to be the main trigger of luminous AGN activity, because SMBH need to accrete substantial fractions of their host galaxy gas (as shown by scaling relations), within durations comparable to dynamical timescales of galaxy centres (Somerville et al. 2008). In the timeline proposed by Hopkins et al, the luminous phase occurs in relatively late merger phases. Luminous AGN stop further infall by radiation pressure and quickly reduce their column densities (Hopkins et al. 2006). In contrast, the faint AGN population is suggested to be dominated by periods before and after peak accretion (Hopkins et al. 2005b). Early merger phases may have enhanced obscuration, both galaxy-scale (Compton-thin) and nuclear (Compton-thin and Compton-thick) (Hopkins et al. 2005a, 2006). Additionally, a substantial part of the faint AGN population is probably associated to secular triggering mechanisms (e.g. Treister et al. 2012). One may therefore argue for a evolutionary AGN life [illustrative lifetimes in brackets] consisting of

- no accretion, and therefore no AGN detection [89%],
- nearby gas leading to obscuration and triggering of a faint AGN [10%], either in the onset of a merger or due to secular events,
- major merger triggering a bright AGN, which immediately clears the vertically extended obscurer but shines for a period of time [1%] before fading.

Such a duty cycle would give rise to the observed obscured fractions (Figure 2) while also respecting the luminosity function of AGN. To summarise, luminous AGN and faint AGN may live in different environments with different gas reservoirs feeding them; therefore unifying the obscuration properties of a luminosity-dependent torus may not be appropriate.

5 COSMOLOGICAL HYDRO-DYNAMIC SIMULATIONS

We now assess the gas content in simulated galaxies. Modern cosmological hydro-dynamic simulations self-consistently evolve galaxies and their processes (star formation, gas accretion, supernova and AGN feedback, etc.) in the context of well-constrained ΛCDM cosmologies. These simulations are constrained in their initial conditions to the baryon density available in the early Universe and are tuned to reproduce the local stellar mass functions. We consider two state-of-the-art cosmological hydro-dynamic simulations which also produce realistic galaxy morphologies. These simulations allow us to look at the spatial distribution of gas inside galaxies.

5.1 Simulation sets

The Evolution and Assembly of Galaxies and their Environment (EAGLE) simulation (Schaye et al. 2015; Crain et al. 2015) reproduces many observed quantities; it reproduces very well the stellar mass function (Furlong et al. 2015b) and size distribution (Furlong et al. 2015a) of galaxies as a function of cosmic time, being tuned to reproduce these at $z = 0$. Further relevant for this work it also produces galaxies with realistic galaxy morphologies (Schaye et al. 2015) and gas contents consistent with observations of CO and HI (Bahe et al. 2015) as well as H_2 (Lagos et al. 2015). This encourages us to look inside simulated galaxies and assess the obscuration provided by them. EAGLE includes black hole particles, which are seeded into dark matter halos exceeding masses of $10^{10} M_\odot$. These black holes are kept near the galaxy centre and may accrete when gas is nearby, in turn activating a feedback mechanism by heating (Schaye et al. 2015). The strength of EAGLE lies in its minimalistic subgrid recipes and the systematic exploration of alterations: Besides the reference model (`L0100N1504_REFERENCE`), a series of simulations with parameter variations have been run to explore the impact of various choices in the subgrid implementations, including the style and strength of supernova feedback, AGN heating and criteria for when stars are formed (Crain et al. 2015).

We also consider Illustris (Vogelsberger et al. 2014b,a), another hydro-dynamic cosmological simulation. This simulation also reproduces many observed quantities; most relevant for this work is that it reproduces the morphology of galaxies, the gas content from CO observations (Vogelsberger et al. 2014b; Genel et al. 2014). The Illustris subgrid models were chosen in consideration of the stellar mass function, star formation history and mass-metallicity relation. However, the weak tuning gave mediocre agreement with regards to the galaxy stellar mass function (Schaye et al. 2015) and size distribution (urlongFURLONG et al. 2015a). On the positive side, the Illustris simulation is based on the AREPO hydrodynamics code which has been shown to reproduce galaxy features well (e.g. Vogelsberger et al. 2012; Nelson et al. 2013). The gas particle resolution in *Illustris* is adaptive, with some cells being as small as 48 pc in the highest resolution simulation (*Illustris-1*) used here, indicating that modern cosmological simulation indeed resolve galaxies into small sub-structures. Illustris also includes black holes, which are created and kept in the grav-

itational potential minimum of galaxies inside halos of mass $M_{\rm DM} > 7.1 \times 10^{10} M_\odot$ (Sijacki et al. 2015).

5.2 Methodology

We first investigate the gas distribution in the reference simulations. We focus on the metal component of gas as O and Fe are, for the relevant obscuring columns and redshifts, the most important elements for photo-electric absorption of X-rays. In galaxy evolution models, the massive end of the existing stellar population expels metals into the galaxy. The metal gas produced per stellar mass is determined by the chosen IMF and the metal yield, with the latter tuned to reproduce the stellar mass function (e.g. Lu et al. 2015). The total metal gas mass residing in galaxies further depends on the chosen feedback models which can expel gas out of the galaxy. Typically the metal gas mass inside galaxies follows a $M_Z : M_\star$ ratio of 1 : 30 to 1 : 100 relation in semi-analytic models at $z = 0 - 3$ (e.g. Croton et al. 2006, 2016); Plots of these models can be found in Appendix A. The crucial remaining question surrounds the arrangement of that gas inside galaxies, as the concentration of gas defines its column density.

We apply ray tracing, starting from the most massive black hole particle of each simulated galaxy (subhalo). From that position, we radiate in random sight-lines all metal gas bound to the subhalo. Along the ray we assign each part the density from the nearest gas particle and finally sum to a total metal column density. This Voronoi tessellation ray tracer can be found at https://github.com/JohannesBuchner/LightRayRider; Catalogues of the obscuration of all considered simulated galaxies are available from the first author on request. We then compute an equivalent hydrogen column density distribution by adopting Wilms et al. (2000) local inter stellar medium (ISM) abundances. This mimics how $N_{\rm H}$ is derived in X-ray observations. For completeness, Appendix B investigates the hydrogen gas and the metallicity of LOS in the simulation. We adopt $h = 0.7$ and work in physical units at redshift slices $z = 0$, 1, 2 and 3. We investigate all galaxy subhaloes with black holes. For each we randomly assign a luminosity according to the SARD of Aird et al. (2012) and use only those with $L(2 - 10\,{\rm keV}) > 10^{42}{\rm erg/s}$. The last step is repeated 400 times to increase the sample size. We therefore do not rely on the instantaneous accretion rates provided by the simulations (see Sijacki et al. 2015; Rosas-Guevara et al. 2016, for Illustris and EAGLE respectively). The effect of adopting these as the selection criterion is discussed later. With the column density distribution for each AGN available, we compute the obscured fraction as a function of column density $N_{\rm H}$ of the simulated population.

5.3 Results

We present the fraction of AGN showing column densities larger than a given $N_{\rm H}$ value in Figure 5. The plot is made in the same fashion as the previous observational Figure 1 and compares against the same observations. In the upper right, $z = 1$ panel of Figure 5, we find that both the EAGLE reference and Illustris simulations produce a negligible number of Compton-thick AGN. This is consistent with the assumption that Compton-thick obscuration is associated with a nuclear obscuration in the vicinity of the accretion disk. We then compare to observations. Downwards-pointing triangles indicate constraints for the obscured fraction of luminous, Compton-thin AGN. Arbitrary additional nuclear obscuration may be included in them, therefore they should be interpreted as upper limits to the galaxy-scale obscuration. We find that the Illustris simulation fulfils these constraints, as it produces very low covering fractions at all obscuring columns. In contrast, the EAGLE reference simulation produces an excess of obscured AGN at $N_{\rm H} = 10^{22}{\rm cm}^{-2}$. This is in violation of observations even when the higher data point from low-luminosity AGN is considered. At higher column densities, the large-scale galaxy gas of the EAGLE reference simulation produces covering fractions consistent with the observations, with no need for a nuclear obscurer up to $N_{\rm H} = 10^{23.5}{\rm cm}^{-2}$. In contrast, Illustris galaxies do not provide column densities of $N_{\rm H} > 10^{23}{\rm cm}^{-2}$ and thus require a nuclear obscurer to explain the observations. The same trends are seen at higher redshifts in the panels of Figure 5. At redshift $z = 0$, both EAGLE and Illustris are consistent with the data points.

5.4 Discussion

We discuss three aspects which affect the results: (1) different sub-grid physics, most notably stronger feedback mechanisms, (2) differences between active and passive galaxies, (3) unresolved substructure of the gas.

The strength of EAGLE is that we can explore how variations of the physics affect the results. The diversity of those predictions is bounded by dotted lines in Figure 5. This indicates that at least some models reproduce fractions in agreement with observation. However it also shows that the simulations are limited in their predictive power, as arbitrary fractions can be produced depending on the input physics. However, we can use observed obscured AGN fractions to exclude simulations which overproduce them, as these observations are apparently quite sensitive to the assumed physics. We focus on the fraction of AGN with $N_{\rm H} > 10^{22}{\rm cm}^{-2}$ at redshift $z = 1$, and compare to EAGLE physics variations in Figure 6. Observations find a fraction around $\sim 30 - 50\%$. We consider any simulation with fractions above 2/3 (right dotted line) as ruled out by observations. This nicely separates the EAGLE physics variations into two groups, one close to the observational constraints, and one significantly over-predicting the fraction of obscured AGN. The EAGLE reference simulation in a large cosmological volume (`L0100N1504_REFERENCE`) belongs to the latter group, as well as the simulation run in medium-size volumes (`L0025N0752_REFERENCE`, `L0025N0752_RECALIBRATED`). We now investigate which changes make the simulation agree better. Crain et al. (2015) presents these variations in detail.

Star formation-related feedback (supernovae, stellar winds, radiation pressure, cosmic rays) was altered in the WeakFB and StrongFB models. The efficiency threshold was modified by factors of 0.5 and 2 respectively, relative to the reference model. Here we find, surprisingly, that both models produce lower obscured fractions than the reference model. Strong feedback leads to underproduction of massive galaxies at $M_\star > 10^{10.5} M_\odot$ (Crain et al. 2015, their Figure 10),

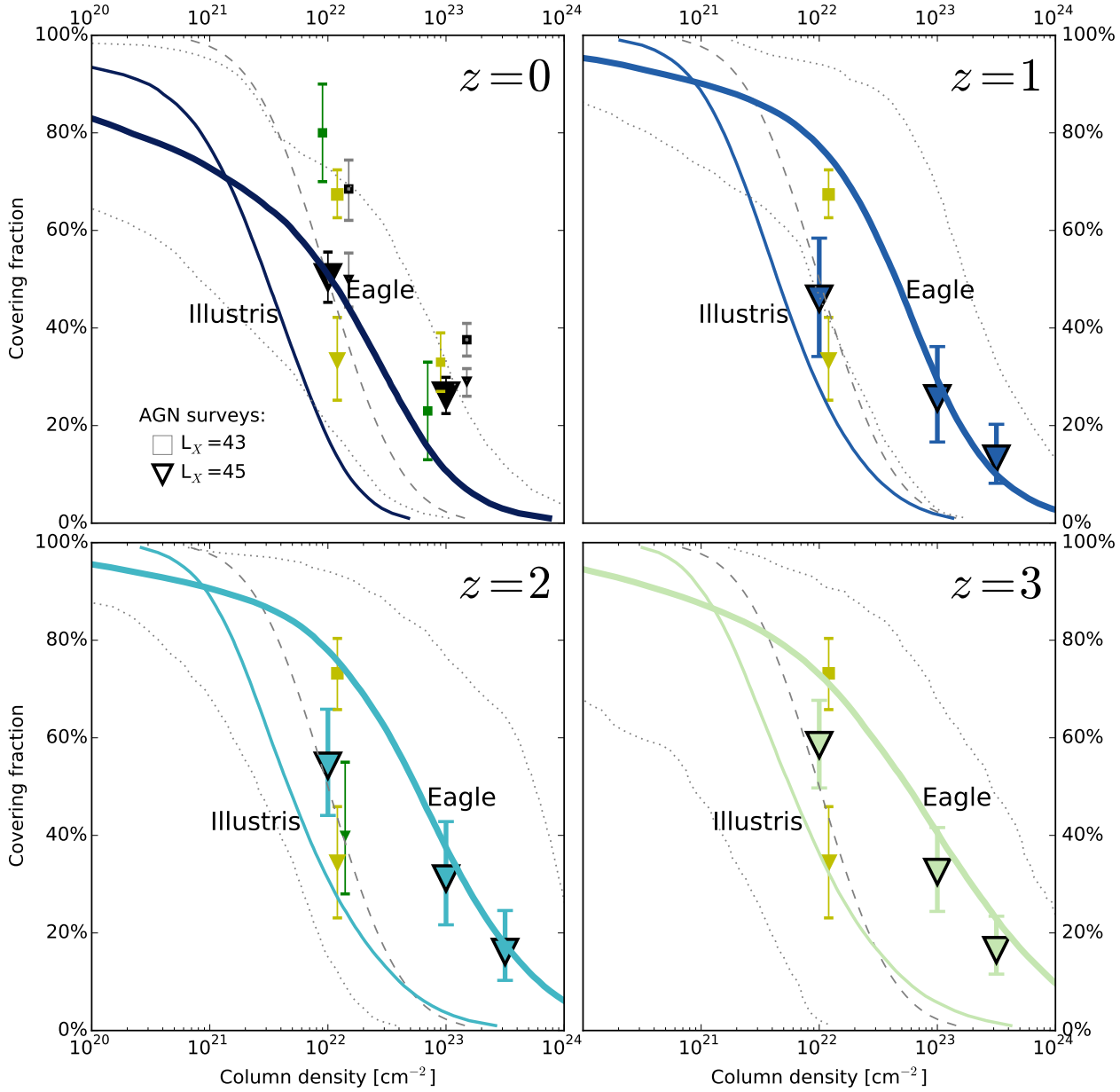

Figure 5. Hydro-dynamic cosmological simulations results for the galaxy-scale gas obscuration of AGN. At various redshift intervals (panels) we show the fraction of AGN (y-axis) that is covered by a given column density $N_{\rm H}$ (x-axis). Curves indicate results from ray-tracing the metal gas. The EAGLE reference simulation (thick line) produces thicker column densities than Illustris (thin line). Data points are the same as in Figure 1. These show fractions from surveys of bright/faint AGN in triangle/square symbols respectively. Since AGN also have a nuclear obscurer, these should be interpreted as upper limits for galaxy gas obscuration. The dashed grey curve (same as in Figure 1) is kept constant across panels for reference.

thereby biasing the galaxy population to small gas masses. It is less clear why the WeakFB produces a small obscured fraction. Presumably the feedback is not sufficient to vertically puff up galaxies, thereby reducing covering fractions. However, these variations can be excluded based on their mismatch with other observations, e.g. the SMF (Crain et al. 2015, their Figure 10).

Next we discuss the effects of feedback from accreting SMBHs. In the EAGLE simulation, there are three parameters which affect the triggering, efficiency and impact of AGN feedback respectively. The equation of state of the ISM can be modified from its reference value (4/3) to 1 (`eos1`). The increased sound speed then increases the accretion onto black holes in the simulation, which increases AGN feedback. Once near the black hole, matter is placed into the black hole with a Bondi accretion formula modified by a viscosity parameter. Increasing the viscosity (`ViscHi`) allows gas to loose angular momentum and accrete more efficiently. Once accreted, the temperature of particles near AGN is increased by $\Delta T = 10^{8.5}$K, stochastically, bringing the gas into the metal cooling regime. Schaye et al. (2015) test the impact of increasing this temperature to $\Delta T = 10^{9}$K (`AGNdT9`). Each

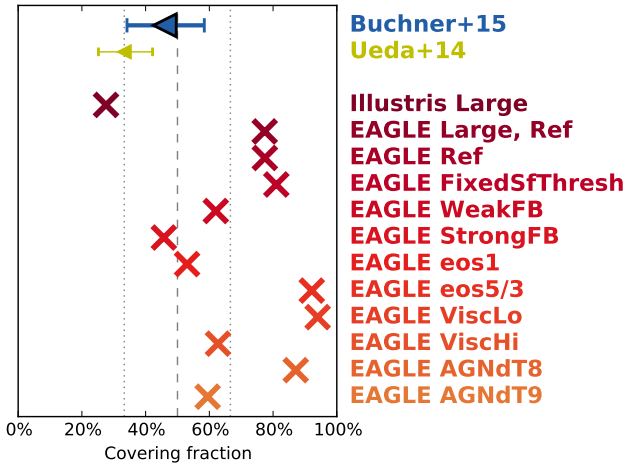

Figure 6. Obscured fractions from various simulations. We compare the fraction of obscured, Compton-thin AGN at $z = 1$ from observations (first two data points) to our observational model (Section 2) and various cosmological simulations.

of these three modification (`eos1`, `ViscHi`, `AGNdT9`) leads to a reduction of the obscured fraction of AGN (see Figure 6), while contrary modifications (`eos5/3`, `ViscLo`, `AGNdT8`) do the opposite. It is worth noting that Schaye et al. (2015) preferred the `AGNdT9` variation over the reference simulation because it better fits soft X-ray observations of cluster gas. We also point out that Illustris uses relative strong feedback, as it implements three different AGN feedback schemes (thermal, kinetic and radiation), whereas EAGLE uses only stochastic heating.

AGN outflows or radiation pressure may decrease the covering fractions momentarily. We have so far considered *all* simulated galaxies and found that they produce high covering fractions. Arguably these fractions are consistent with the covering fraction of low-luminosity AGN. Therefore, one could propose that AGN feedback at high luminosities modifies the galaxy in such way that covering fractions are reduced. Apriori this proposal appears unlikely, because nuclear gas should be affected first. Additionally, studies comparing the morphology of active and passive galaxies have found little evidence that these are different, by comparing appearances with asymmetry and concentration measures (Grogin et al. 2003, 2005; Pierce et al. 2007; Gabor et al. 2009; Kocevski et al. 2012) or visual classification (Kocevski et al. 2012). Indeed, our results remain unchanged if in the EAGLE reference simulation we only consider simulated galaxies with instantaneous black hole accretion rates corresponding to $L(2-10\,\mathrm{keV}) > 10^{42}\mathrm{erg/s}$, assuming a radiative efficiency of 10% and bolometric corrections of Marconi et al. (2004). In fact, since active galaxies are preferentially gas-rich, star-forming galaxies in that simulation, the average column density is higher by a factor of 2, which increases the discrepancy.

Clumpy ISM may decrease the covering fractions. For instance the galactic ISM is structured into parsec-size clumps with filling factors of 1% (Cox 2005). Such clumps could not be resolved by simulations. However, as a LOS passes through large distances of the ISM (1 – few kiloparsecs), this clumpiness averages out. Additionally, clumpiness would effectively only redistribute the obscured fraction to both lower and higher column densities, potentially violating the constraints of higher column densities. There are also differences in the hydrodynamics code schemes and their accuracy. However, these are less important than the chosen sub-grid models (J. Shaye, priv. comm., see Scannapieco et al. 2012; Schaller et al. 2015; Cui & Power 2016; Sembolini et al. 2016) in the present non-classical SPH simulations.

To summarise, our obscured fraction diagnostic is a highly sensitive test of feedback recipes. It can easily rule out feedback models already at early times (e.g. $z = 3$) in the simulations, if they produce very high fractions of obscured AGN.

6 CONCLUSIONS

Using only observational relations, we predict the covering fractions of galaxy-scale gas as relevant for the AGN population. Our findings can be summarised as follows:

(i) Galaxy-scale gas does not provide Compton-thick lines of sight.
(ii) Galaxy-scale gas covers substantial fractions of the SMBH population at $N_\mathrm{H} \approx 10^{22-23.5}\mathrm{cm}^{-2}$, sufficient to explain the observed luminosity-independent baseline obscuration.

We therefore conclude that heavily obscured AGN are associated with nuclear obscuration, and propose the value $N_\mathrm{H} = 10^{23.5}\mathrm{cm}^{-2}$ as a demarcation line singling out the nuclear obscurer.

We subtracted the galaxy-scale obscuration and concluded regarding the remaining nuclear obscurer, that

(i) a nuclear Compton-thick obscurer with $\sim 35\%$ covering is necessary.
(ii) a nuclear Compton-thin obscurer is necessary for some combinations of luminosity/black hole mass.

The result is formalised into a semi-analytic model for cosmological simulations, called PuffedTorus (Section 4.2). The cartoon of Figure 4 illustrates a possible physical scenario for these three, distinct obscuring components.

We also investigated the inside of simulated galaxies from state-of-the-art hydro-dynamic, cosmological simulations and apply ray-tracing from their black holes. Some of these simulations produce obscured fractions from their metal gas which is consistent with observed populations. However, the results are highly sensitive to the adopted feedback models and therefore lack predictive power. We therefore suggest the Compton-thin obscured AGN fraction as a diagnostic to rule out feedback models. This diagnostic which can be applied already at early cosmic times ($z = 2 - 3$).

ACKNOWLEDGEMENTS

JB thanks Antonis Georgakakis and Dave Alexander for insightful conversations. JB thanks Joop Schaye for detailed comments pertaining the hydrodynamic simulations work. JB thanks Klaus Dolag, Sergio Contreras and Torsten Naab for conversations about hydro-dynamic simulations.

References

Aird J., et al., 2010, MNRAS, 401, 2531
Aird J., et al., 2012, ApJ, 746, 90
Aird J., et al., 2013, ApJ, 775, 41
Aird J., Coil A. L., Georgakakis A., Nandra K., Barro G., Perez-Gonzalez P. G., 2015, preprint, (arXiv:1503.01120)
Bahe Y. M., et al., 2015, preprint, (arXiv:1511.04909)
Barger A. J., Cowie L. L., 2005, ApJ, 635, 115
Bongiorno A., et al., 2012, MNRAS, 427, 3103
Brightman M., Nandra K., 2011, MNRAS, 414, 3084
Brightman M., Nandra K., Salvato M., Hsu L.-T., Aird J., Rangel C., 2014, MNRAS, 443, 1999
Buchner J., et al., 2015, ApJ, 802, 89
Burlon D., Ajello M., Greiner J., Comastri A., Merloni A., Gehrels N., 2011, ApJ, 728, 58
Ciotti L., Ostriker J. P., 2001, ApJ, 551, 131
Cox D. P., 2005, ARA&A, 43, 337
Crain R. A., et al., 2015, MNRAS, 450, 1937
Croton D. J., et al., 2006, MNRAS, 365, 11
Croton D. J., et al., 2016, preprint, (arXiv:1601.04709)
Cui W., Power C., 2016, MNRAS, 458, 4052
Dickey J. M., Lockman F. J., 1990, ARA&A, 28, 215
Ebrero J., et al., 2009, A&A, 493, 55
Elitzur M., 2006, New Astron. Rev., 50, 728
Elitzur M., Netzer H., 2016, preprint, (arXiv:1603.04909)
Enoki M., Ishiyama T., Kobayashi M. A. R., Nagashima M., 2014, ApJ, 794, 69
Fanidakis N., et al., 2012, MNRAS, 419, 2797
Furlong M., et al., 2015a, preprint, (arXiv:1510.05645)
Furlong M., et al., 2015b, MNRAS, 450, 4486
Gabor J. M., et al., 2009, ApJ, 691, 705
Genel S., et al., 2014, MNRAS, 445, 175
Goulding A. D., Alexander D. M., 2009, MNRAS, 398, 1165
Grogin N. A., et al., 2003, ApJ, 595, 685
Grogin N. A., et al., 2005, ApJ, 627, L97
Hasinger G., Miyaji T., Schmidt M., 2005, A&A, 441, 417
Hirschmann M., Naab T., Somerville R. S., Burkert A., Oser L., 2012, MNRAS, 419, 3200
Hirschmann M., Dolag K., Saro A., Bachmann L., Borgani S., Burkert A., 2014, MNRAS, 442, 2304
Hoenig S. F., 2013, preprint, (arXiv:1301.1349)
Hönig S. F., Beckert T., 2007, MNRAS, 380, 1172
Hopkins P. F., Hernquist L., Cox T. J., Di Matteo T., Martini P., Robertson B., Springel V., 2005a, ApJ, 630, 705
Hopkins P. F., Hernquist L., Cox T. J., Di Matteo T., Robertson B., Springel V., 2005b, ApJ, 630, 716
Hopkins P. F., Hernquist L., Cox T. J., Di Matteo T., Robertson B., Springel V., 2006, ApJS, 163, 1
Ilbert O., et al., 2013, A&A, 556, A55
Kalberla P. M. W., Burton W. B., Hartmann D., Arnal E. M., Bajaja E., Morras R., Pöppel W. G. L., 2005, A&A, 440, 775
Kelly B. C., Shen Y., 2013, ApJ, 764, 45
King A. R., Pringle J. E., 2006, MNRAS, 373, L90
Kocevski D. D., et al., 2012, ApJ, 744, 148
La Franca F., et al., 2005, ApJ, 635, 864
Lagos C. d. P., et al., 2015, MNRAS, 452, 3815
Lu Y., Mo H. J., Lu Z., 2015, preprint, (arXiv:1504.02109)
Lusso E., et al., 2013, ApJ, 777, 86
Madau P., Dickinson M., 2014, ARA&A, 52, 415
Maiolino R., Rieke G. H., 1995, ApJ, 454, 95
Maiolino R., Shemmer O., Imanishi M., Netzer H., Oliva E., Lutz D., Sturm E., 2007, A&A, 468, 979
Marconi A., Risaliti G., Gilli R., Hunt L. K., Maiolino R., Salvati M., 2004, MNRAS, 351, 169
Markowitz A. G., Krumpe M., Nikutta R., 2014, MNRAS, 439, 1403
Matt G., 1997, Mem. Soc. Astron. Italiana, 68, 127
Matt G., 2000, A&A, 355, L31
Molinari S., et al., 2011, ApJ, 735, L33
Morris M., Serabyn E., 1996, ARA&A, 34, 645
Mullaney J. R., et al., 2015, MNRAS, 453, L83
Muzzin A., et al., 2013, ApJ, 777, 18
Nelson D., Vogelsberger M., Genel S., Sijacki D., Kereš D., Springel V., Hernquist L., 2013, MNRAS, 429, 3353
Netzer H., Lani C., Nordon R., Trakhtenbrot B., Lira P., Shemmer O., 2016, ApJ, 819, 123
Oh K., Yi S. K., Schawinski K., Koss M., Trakhtenbrot B., Soto K., 2015, ApJS, 219, 1
Perley D. A., et al., 2016, ApJ, 817, 8
Pierce C. M., et al., 2007, ApJ, 660, L19
Pontzen A., et al., 2010, MNRAS, 402, 1523
Prieto M. A., Mezcua M., Fernández-Ontiveros J. A., Schartmann M., 2014, MNRAS, 442, 2145
Ricci C., Ueda Y., Koss M. J., Trakhtenbrot B., Bauer F. E., Gandhi P., 2016, preprint, (arXiv:1603.04852)
Risaliti G., Maiolino R., Salvati M., 1999, ApJ, 522, 157
Rosario D. J., et al., 2011, preprint, (arXiv:1110.3816)
Rosario D. J., et al., 2013, ApJ, 771, 63
Rosas-Guevara Y., Bower G. R., Schaye J., McAlpine S., Dalla-Vecchia C., Frenk S. C., Schaller M., Theuns T., 2016, preprint, (arXiv:1604.00020)
Santini P., et al., 2012, A&A, 540, A109
Scannapieco C., et al., 2012, MNRAS, 423, 1726
Schaller M., Dalla Vecchia C., Schaye J., Bower R. G., Theuns T., Crain R. A., Furlong M., McCarthy I. G., 2015, MNRAS, 454, 2277
Schaye J., et al., 2015, MNRAS, 446, 521
Schulze A., Wisotzki L., 2010, A&A, 516, A87
Schulze A., et al., 2015, MNRAS, 447, 2085
Sembolini F., et al., 2016, MNRAS,
Sijacki D., Vogelsberger M., Genel S., Springel V., Torrey P., Snyder G. F., Nelson D., Hernquist L., 2015, MNRAS, 452, 575
Silverman J. D., et al., 2008, ApJ, 679, 118
Somerville R. S., Hopkins P. F., Cox T. J., Robertson B. E., Hernquist L., 2008, MNRAS, 391, 481
Stalevski M., Ricci C., Ueda Y., Lira P., Fritz J., Baes M., 2016, MNRAS,
Tacconi L. J., et al., 2013, ApJ, 768, 74
Treister E., et al., 2004, ApJ, 616, 123
Treister E., Schawinski K., Urry C. M., Simmons B. D., 2012, ApJ, 758, L39
Ueda Y., Akiyama M., Ohta K., Miyaji T., 2003, ApJ, 598, 886
Ueda Y., Akiyama M., Hasinger G., Miyaji T., Watson M. G., 2014, ApJ, 786, 104
Vogelsberger M., Sijacki D., Kereš D., Springel V., Hernquist L., 2012, MNRAS, 425, 3024
Vogelsberger M., et al., 2014a, MNRAS, 444, 1518
Vogelsberger M., et al., 2014b, Nature, 509, 177
Wada K., 2012, ApJ, 758, 66
Wada K., 2015, preprint, (arXiv:1509.00576)
Wilms J., Allen A., McCray R., 2000, ApJ, 542, 914
Winter L. M., Mushotzky R. F., Reynolds C. S., Tueller J., 2009, ApJ, 690, 1322

APPENDIX A: THE GAS MASS INSIDE GALAXY

Important constraints on how much gas resides in galaxies can be drawn from cosmological simulations. Such simulations evolve the matter density available at the Big Bang into collapsing bound structures. Semi-analytic models, relying on dark matter haloes from dark matter N-body sim-

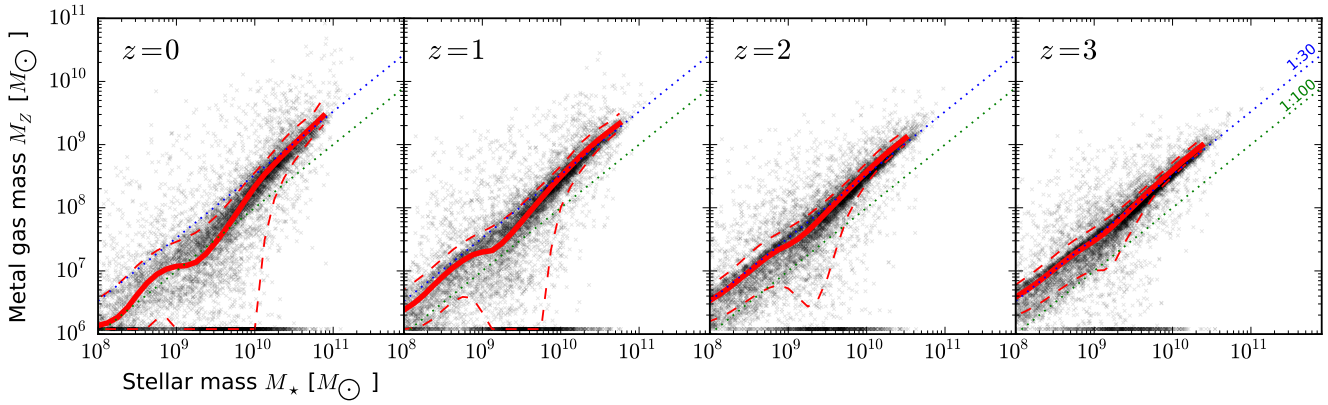

Figure 1. The metal gas mass in galaxies according to the SAGE semi-analytic model. Red indicates the median, while dashed lines are the 1σ-equivalent quantiles. The ratio of metal gas to stellar mass lies between $1:30$ and $1:100$.

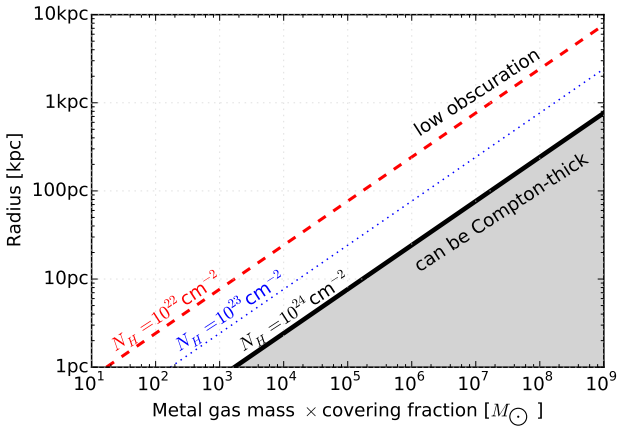

Figure A1. X-ray obscuration a given metal gas mass can reach. A obscurer of column density N_H outside a radius R has a minimum metal gas mass limit M_Z (lines). For example, a $M_Z = 10^9 M_\odot$ gas mass has to be brought withing 100pc to completely enshroud a region with Compton-thick column densities. Keep in mind that such masses are only found in very massive galaxies ($M_\star > 3 \cdot 10^{10} M_\odot$, see Figure 1).

ulations have been highly successful in reproducing many features of galaxies, including the stellar mass function of galaxies and their colour distribution (Croton et al. 2006; Somerville et al. 2008; Hirschmann et al. 2012; Fanidakis et al. 2012). As an illustrative case, we consider the model of Croton et al. (2016). Figure 1 plots the metal gas mass (the X-ray obscurer) present as a function of galaxy stellar mass. The median (red curve) falls consistently in the 1:30 to 1:100 range for the ratio of metal gas mass to stellar mass. With AGN host galaxies primarily drawn around the $M_\star = 10^{10-11} M_\odot$ regime, the total gas available to obscure a central point source is about $M_Z \sim 10^9 M_\odot$. The Illustris simulation shows very similar results at $z = 1-3$ obeying the same gas ratios. However at $z = 0$, the high-mass end is lacks gas due to the strong feedback implemented in that simulation.

We present a simple calculation to show that Compton-thick column densities, i.e. $N_\mathrm{H} > 1.5 \times 10^{24} \mathrm{cm}^{-2}$) can not be achieved by accumulating the galaxy gas over several kpc. In X-ray spectral analysis, the equivalent hydrogen column density N_H is usually computed assuming solar abundances. To mimic this, we convert the metal mass in particles to the number of hydrogen atoms assuming solar mass fractions of the nearby ISM from Wilms et al. (2000):

$$n_\mathrm{H} = \left.\frac{f_\mathrm{X}}{f_\mathrm{Z}}\right|_\mathrm{solar} \times \frac{\rho_\mathrm{Z}}{m_\mathrm{H}}$$

Inserting numbers including the hydrogen mass m_H we find

$$n_\mathrm{H} = 0.737 \times 10^{22} \mathrm{cm}^{-2} \frac{1}{1\mathrm{kpc}} \times \frac{\rho_\mathrm{Z}}{10^6 M_\odot \mathrm{kpc}^{-3}}.$$

For example, a 1kpc ray in a region of metal gas density $10^6 M_\odot/\mathrm{kpc}^3$ results in a measured column density of $N_\mathrm{H} \approx 10^{22} \mathrm{cm}^{-2}$.

The gas inside a galaxy may be arranged in a multitude of ways to achieve a covering with column density N_H. If we consider only gas *outside* a certain radius R, the most effective obscurer, i.e. the one with the least mass but complete covering, is an infinitely thin shell at that radius R. Its mass is easily computed as

$$M_\mathrm{H}(N_\mathrm{H}, > R) = 4\pi \cdot R^2 \times N_\mathrm{H} \times m_\mathrm{H}.$$

Converting to metals using the factor $\left.\frac{f_\mathrm{Z}}{f_\mathrm{X}}\right|_\mathrm{solar}$ and expressing in conventional units, this limit is

$$M_\mathrm{Z}(N_\mathrm{H}, > R) = 2.6 \times 10^9 M_\odot \cdot \frac{N_\mathrm{H}}{1.5 \times 10^{24} \mathrm{cm}^{-2}} \cdot \left(\frac{R}{1\mathrm{kpc}}\right)^2.$$

Therefore, a metal mass larger than $2.6 \times 10^9 M_\odot$ is required to create a Compton-thick obscurer outside the central 1kpc. Or equivalently, a metal mass of $2.6 \times 10^9 M_\odot$ has to be brought to the central kpc to act as a Compton-thick obscurer. Note that this mass limit scales with the covering factor; for example obscuration of 10% of the sky requires 10% of the mass. This simple limit is shown for several levels of obscuration in Figure A1. Risaliti et al. (1999) already noted that such large masses at radii further than a few 10 pc are ruled out in NGC1068 and Circinus because they would gravitationally dominate the central region.

Combining this simple limit with the masses of Figure 1, we can now conclude that galaxies simply do not have the required gas to provide Compton-thick obscurers with

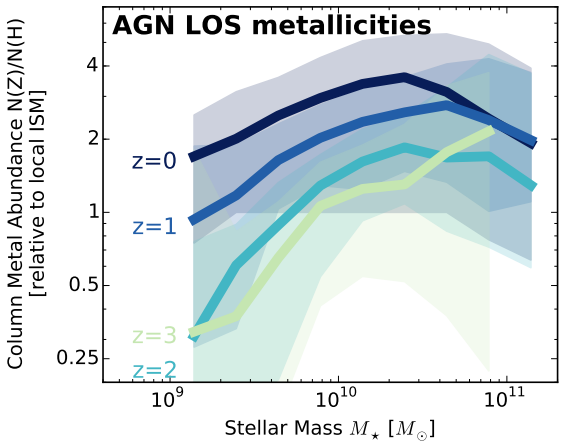

Figure B1. LOS column abundances to AGN. In the EAGLE reference simulation, hydrogen and metal gas densities were integrated along random sightlines from the central black hole to the edge of the host galaxy; the ratio is presented. Curves present the median, while the shaded regions represent the 1σ scatter in the population. LOS metallicities are in general elevated compared to n the local ISM and show a stellar-mass dependence.

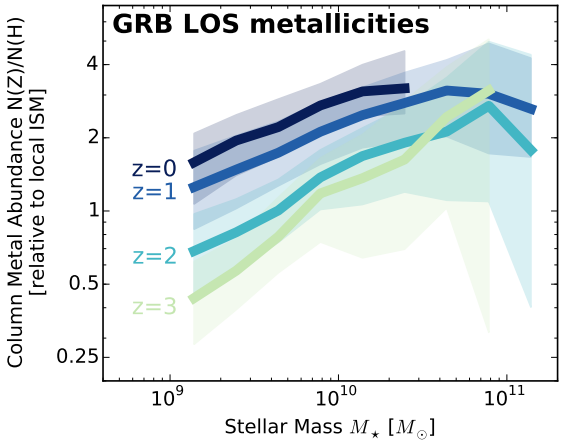

Figure B2. LOS column abundances to GRBs. Same as in Figure B1, but sightlines started from the from the densest regions.

substantial covering factors outside the central 1kpc. Admittedly, this is a weak constraint. However the result holds independently of the geometry of the gas, the type of galaxy and is also applicable to mergers. As an example, lets consider that a $M_\star = 10^9 M_\odot$ merges into a $M_\star = 10^{10} M_\odot$ galaxy (minor merger), and lets assume that all of its gas ($M_Z \approx 10^7 M_\odot$) is made available. That entire amount of gas must land within 100pc of the AGN in order to completely enshroud in Compton-thick columns. More quantitative conclusions depend on the geometrical distribution of the gas in the galaxy. We analyse the galaxies produced by hydrodynamic simulations in Section 5.

APPENDIX B: METALLICITY OF SIGHTLINES TO AGN AND GRB

This paper focused on metal column densities, not hydrogen column densities. We now consider the hydrogen column densities in the reference EAGLE simulation. Our goal is to investigate whether and how they are different from the usually assumed local ISM metallicities in X-ray observation of high-redshift sources. Bahe et al. (2015) investigated already the hydrogen masses and surface densities of EAGLE galaxies and found good agreement with observations. Here we investigate the abundance in random sightlines for AGN. The top panel of Figure B2 presents the metal abundance N_Z/N_H relative to local ISM abundances of Wilms et al. (2000) as a function of galaxy mass for AGN. In general, approximately solar abundances are predicted as the LOS crosses the host galaxy. The abundance increases over cosmic time as metals build up. Also, there is the usual mass-dependent increase in metallicity. This effect is less prominent in AGN sightlines (Figure B1) which always end in the metal-rich centre of galaxies.

For completeness we also present the expected metallicities for GRB sightlines in Figure B2. For low stellar mass hosts at high redshift, they are expected to be sub-solar. These hosts dominate the observed host distribution (see e.g., Perley et al. 2016), and therefore sub-solar metallicities are to be expected in LGRB afterglow spectroscopy. For research on the optical absorption of GRBs by HI we refer to the simulations of Pontzen et al. (2010).